

# Enhanced speed sensorless control of IPMSM using integral synergetic observer

Measurement and Control  
1–15

© The Author(s) 2025

Article reuse guidelines:

sagepub.com/journals-permissions

DOI: 10.1177/00202940241312846

journals.sagepub.com/home/mac



Soufyane Boudouani<sup>1</sup> , Adil Yahdou<sup>1</sup>, Habib Benboughenni<sup>2</sup> ,  
Zinelaabidine Boudjema<sup>1</sup>, Mishari Metab Almalki<sup>3</sup> and  
Thamer AH Alghamdi<sup>3,4</sup>

## Abstract

Owing to the benefits of uncomplicated design, compact dimensions, and superior power density, interior permanent magnet synchronous motors (IPMSMs) have garnered the attention of numerous researchers, both nationally and internationally. Nevertheless, conventional IPMSM models incorporating sensors, encoders, and additional apparatus often incur substantial equipment expenses and heavily depend on sensor accuracy for effective control. Consequently, the pursuit of sensorless control has emerged as a prominent trend in the domain of IPMSM control. In this work, a new sensorless control based on an integral synergetic observer (ISO) for an IPMSM is presented. The suggested observer has been developed to overcome the challenges posed by conventional observers, such as fragility against various disturbances, and establishing a sensorless control scheme capable of easily integrating into a modern application like electric vehicles. A comparison through numerical simulation tests using MATLAB software, between the proposed observer and the classic Luenberger observer (LO) clearly showed its qualities and its great importance. Notably, the ISO achieves improved performance metrics, such as the integral absolute error (IAE), integral square error (ISE), and integral time absolute error (ITAE). In low-speed control tests, the proposed ISO reduced the IAE by 56.90%, the ITAE by 55.83%, and the ISE by 75.82% compared to the LO.

## Keywords

Interior permanent magnet synchronous motors, speed sensorless, integral synergetic observer, Luenberger observer, electric vehicles

Date received: 6 April 2024; accepted: 16 December 2024

## Introduction

The interior permanent magnet synchronous motor (IPMSM) is widely used in various drive applications, including industrial facilities and electric vehicles, where high performance, power factor, and efficiency are essential. IPMSMs offer the advantage of generating high torque with compact rotor sizes due to saliency, which enables both magnetic and reluctance torque production.<sup>1,2</sup> To effectively drive an AC motor like the IPMSM, position, and rotor speed information are typically obtained from a linear encoder. However, linear encoders are generally less reliable and more costly than their counterparts in rotating machines, with costs increasing as the track length grows. This poses challenges in applications such as railway traction and long-track motion systems, where the linear encoder is frequently exposed to potentially damaging environmental factors (e.g. sunlight, humidity, mechanical stress).

These conditions underscore the importance of implementing robust sensorless methods.<sup>3,4</sup>

In recent decades, significant research has focused on developing sensorless control techniques for AC drives, which are typically categorized into high-

<sup>1</sup>Department of Electrical Engineering, Laboratoire Génie Electrique et Energies Renouvelables (LGEER), Hassiba Benbouali University of Chlef, Chlef, Algeria

<sup>2</sup>Department of Electrical Engineering, LAAS Laboratory, National Polytechnic School of Oran-Maurice Audin, Oran El M'naouer, Algeria

<sup>3</sup>Electrical Engineering Department, School of Engineering, Al-Baha University, Al-Baha, Saudi Arabia

<sup>4</sup>Wolfson Centre for Magnetism, School of Engineering, Cardiff University, Cardiff, UK

### Corresponding author:

Soufyane Boudouani, Department of Electrical Engineering, Laboratoire Génie Electrique et Energies Renouvelables (LGEER), Hassiba Benbouali University of Chlef, Chlef 02000, Algeria.

Emails: s.boudouani22@univ-chlef.dz; thamerladnan@bu.edu.sa



Creative Commons CC BY: This article is distributed under the terms of the Creative Commons Attribution 4.0 License (<https://creativecommons.org/licenses/by/4.0/>) which permits any use, reproduction and distribution of the work without

further permission provided the original work is attributed as specified on the SAGE and Open Access pages (<https://us.sagepub.com/en-us/nam/open-access-at-sage>).

frequency signal injection methods and fundamental model-based approaches.<sup>5,6</sup> High-frequency signal injection relies on auxiliary signals to extract motor state information, while model-based methods leverage mathematical models to infer unknown parameters based on available data. This classification has yielded a range of methods shaped by different system models, application constraints, and solution methodologies.<sup>7,8</sup>

The Extended Kalman Filter (EKF) stands as a foundational technique, merging Kalman filtering principles with nonlinear models to estimate motor states, such as rotor position and speed, with high accuracy even amidst measurement noise. Its capacity to manage uncertainties and system nonlinearities has solidified EKF's role in sensorless control applications.<sup>9,10</sup>

Another widely employed approach is the model reference adaptive system (MRAS), which utilizes an adaptive observer to estimate essential motor parameters (e.g. rotor flux and speed) by comparing the actual motor response to a reference model. MRAS is particularly valued for its adaptability to parameter variations and robustness against external disturbances, making it a practical choice in real-world implementations.<sup>11,12</sup>

Similarly, the sliding mode observer (SMO) is recognized for its robustness, employing sliding surfaces to minimize estimation errors and accurately track motor behavior under challenging conditions. This technique has gained broad application across various motor types, underscoring its reliability and performance in sensorless control.<sup>13,14</sup>

Although model predictive control (MPC) primarily serves as a control strategy, it often integrates observers for precise state estimation, enabling optimized control actions through predictions of future motor dynamics. MPC's inclusion of state estimation techniques enhances its utility in sensorless applications by ensuring high control accuracy.<sup>15-17</sup>

Finally, the extended state observer (ESO) offers advanced capabilities by estimating both system states and disturbances. This observer is particularly advantageous in environments with load variations and parameter uncertainties, contributing to increased robustness and enhanced performance in sensorless control.<sup>18,19</sup>

Together, these techniques significantly contribute to advancing sensorless control by enhancing adaptability, accuracy, and robustness in motor control applications.

The Luenberger observer (LO), also known as the Luenberger state observer, has emerged as a powerful tool for estimating unmeasured states in dynamic systems. The LO provides an elegant solution by reconstructing the system's internal states based on available measurements. Its key advantages lie in simplicity, ease of implementation, and computational efficiency. However, there is a notable drawback: the LO's vulnerability to disturbances and parameter uncertainties, limits its robustness in practical applications.<sup>20-23</sup> That's why, we delve into the theory, benefits, and challenges associated with this widely used observer.

Table 1 presents various proposed solutions for improving sensorless control in IPMSM drives found in the literature, including the high-frequency (HF) method, the adaptive robust unscented Kalman filter (UKF), the extended flux (EF) model-based proportional-integral (PI) observer, the fuzzy logic (FL) observer, and other techniques.

In this paper, we propose to extend the theory of LOs by a new nonlinear approach based on the integral synergetic technique (IST). This suggested technique is a development and extension of the classical synergetic control (SC) which remains one of the robust nonlinear control techniques, as demonstrated in Benbouhenni.<sup>31</sup> Compared to the sliding mode control (SMC) method, the SC approach is simple, uncluttered, and considerably lessens chattering. In Benbouhenni et al.<sup>32</sup> the authors suggest a novel method of SC based on the integral of the macro-variable. Double-loop control is the foundation of this novel design, which increases the effectiveness and robustness of the control. Furthermore, the designed IST law is robust to changes in the system's parameters.

The main contributions of this study are summarized as follows:

- The development of a robust and efficient sensorless control scheme for IPMSM using the integral synergetic observer (ISO).
- A comparative study between the LO and ISO applied to IPMSM under normal and exceptional conditions.
- Ensuring robustness and accurate reference tracking in the presence of various disturbances.
- Enhancing sensorless control performance in low-speed scenarios.
- Addressing the limitations of the classical LO technique.
- Minimizing the ISE, IAE, overshoot, speed drop, and ITAE compared to LO.

The rest of the paper is organized as follows: Section 2 provides a concise overview of the mathematical structure of the IPMSM. Section 3 elaborates on the definition of the traditional LO approach used for its estimation. Section 4 introduces the designed ISO, which addresses the shortcomings of the conventional observer, with detailed explanations. Subsequently, simulation results are illustrated under various conditions: speed change, low-speed, no load, parameter variation, and load change. These results showcase the reliability and precision of the designed sensorless control approach. Finally, concluding remarks are provided in the last section of the paper.

## IPMSM model

As shown in Figure 1, an IPMSM is formed of a stator, rotor, windings, permanent magnets, and a shaft. In

**Table 1.** Some published paper addressing the sensorless control of IPMSM.

References	Techniques	Contributions	Limitations
Li et al. <sup>24</sup>	HF signal injection method.	The paper introduces a HF response current direct demodulation method for sensorless IPMSM control, incorporating mean-value extraction, self-demodulation, and online cross-saturation angle compensation to improve low-speed accuracy and efficiency.	The study is limited by sensitivity to parameter variations, complex online compensation, and diminished effectiveness at high speeds from decreasing HF signal strength.
Ding et al. <sup>25</sup>	Adaptive robust UKF.	The paper presents a sensorless control method for SPMSMs using an adaptive robust UKF for accurate state estimation, improving robustness and reducing reliance on physical sensors.	Susceptibility to system noise and measurement gross errors, which the adaptive robust UKF aims to mitigate but may not completely eliminate.
Salman and Yilmaz <sup>26</sup>	EF model-based PI observer.	This article proposes a new sensorless control method for IPMSMs using an EF model-based PI observer, optimized with linear quadratic regulator (LQR) gains, significantly enhancing low-speed performance and robustness in washing machine applications under varying load conditions.	Less effective in scenarios with extremely high-speed operations or significant parameter variations, and it primarily focuses on low-speed performance, potentially limiting its applicability to broader industrial applications.
Wu and Lin <sup>27</sup>	Adaptive interconnected state observer.	The paper presents an adaptive interconnected observer for sensorless speed control of permanent magnet linear synchronous motors, integrating a Kalman filter and backstepping control (BC) to enhance robustness against variable conditions.	The approach targets low-speed operations but may struggle with high-speed scenarios or rapid parameter changes, and its adaptability to complex disturbances in real-world applications is unproven.
Chen and Wu <sup>28</sup>	Pseudo-random HF signal injection (PR-HFSI) in the zero-low speed range.	This paper proposes a stator flux-oriented sensorless direct torque and flux control method for IPMSMs using PR-HFSI technique, eliminating extra transformations. It reduces HF noise, analyzes optimal injection frequencies, and validates the approach experimentally on a 60 kW IPMSM.	The approach shows promise at low speeds, yet may face high-speed challenges in industrial settings; noise reduction is improved, but real-world effectiveness is unconfirmed.
Jiang et al. <sup>29</sup>	Integral terminal sliding mode controller (TSMC). Extended state observer (ESO).	The authors propose a modified integral sliding mode control (ISMC) with a continuous reaching law to reduce chattering and singularity issues. Incorporating an extended state observer (ESO) enhances disturbance rejection, leading to a robust and fast control method ensuring high precision.	The proposed method reduces but does not fully eliminate chattering and requires extensive parameter tuning, making the control design complex and demanding for optimal performance adjustments.
Ye <sup>30</sup>	Fuzzy sliding mode observer	Chattering suppression. Improved dynamic performance. Robustness.	Complexity. Low-speed issues.

IPMSMs, the  $d$ - $q$  reference frame is regularly used to facilitate calculations of current and voltage. The magnetic field direction of the rotor acts as the  $d$ -axis, which runs along the magnetic pole centerline of the rotor. The  $q$  axis, on the vertical bisector between two adjacent magnetic poles, is defined as the direction orthogonal to the rotor magnetic field. To reduce

demagnetization in the field weakening (FW) working zone, a V-shaped technique is used. Furthermore, the reluctance torque produced by the difference in  $d$ -axis and  $q$ -axis inductances is favorable for increasing speed in the FW working zone.<sup>33</sup>

The model of the IPMSM is given in equations (1) and (2)<sup>34</sup>:

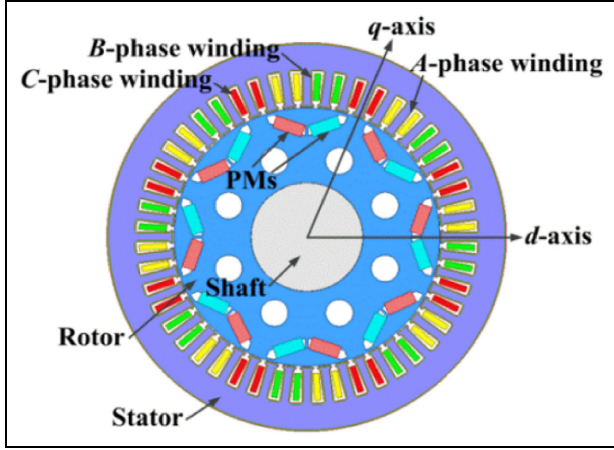


Figure 1. Structure of the IPMSM.<sup>33</sup>

$$\frac{di_d}{dt} = -\frac{R_s}{L_d}i_d + \frac{L_q}{L_d} \cdot w \cdot i_q + \frac{V_d}{L_d} \quad (1)$$

$$\frac{di_q}{dt} = -\frac{R_s}{L_q}i_q - \frac{L_d}{L_q} \cdot w \cdot i_d - \frac{\psi_f w}{L_q} + \frac{V_q}{L_q} \quad (2)$$

where  $i_d$  and  $i_q$  represent the stator currents along the  $d$  and  $q$  axes, respectively;  $V_d$  and  $V_q$  denote the stator voltages along the  $d$  and  $q$  axes;  $R_s$  signifies the stator resistance;  $L_d$  and  $L_q$  denotes the direct and quadrature stator inductance;  $\psi_f$  represents the flux linkage; and  $w$  represents the rotor angular velocity.

The expression for the mechanical equation of the IPMSM is given by equation (3).

$$\frac{dw}{dt} = \frac{T_e}{J} - \frac{f}{J}w - \frac{C_r}{J} \quad (3)$$

where,  $T_e$  represents the electromagnetic torque,  $f$  denotes the viscous friction coefficient,  $J$  is the inertia, and  $C_r$  represents the load torque.

When the machine operates without application of the load torque, equation (3) becomes:

$$\frac{dw}{dt} = \frac{T_e}{J} - \frac{f}{J}w \quad (4)$$

Equation (5) presents the expression for electromagnetic torque.

$$T_e = \frac{3}{2}p(\psi_f i_q + (L_d - L_q)i_d i_q) \quad (5)$$

where,  $p$  represents the number of pole pairs.

### Conventional speed and position estimations for IPMSM

The LO proves beneficial for systems with measurements that aren't excessively noisy. Additionally, the

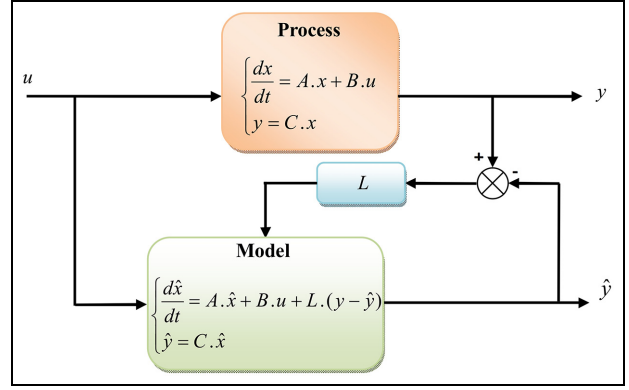


Figure 2. Block diagram of the LO.

LO acknowledges the nonlinear state of the IPMSM model. When a system is observable, Figure 2 can be employed to depict the observer. In our model, we omitted the mechanical sensors and employed a second-order LO or reduced-order observer to calculate the load torque and speed, assuming no influence from noise on the system operation (operating in a deterministic environment). We are familiar with the following expression for the torque in an IPMSM<sup>35,36</sup>:

$$T_e = \frac{3}{2} \cdot p \cdot (\psi_f \cdot i_q) \quad (6)$$

By substituting equation (6) into equation (3), we obtain the mechanical speed equation as follows:

$$\frac{dw}{dt} = \frac{1}{J} \left( \frac{3}{2} \cdot p \cdot (\psi_f \cdot i_q) - C_r - f \cdot w \right) \quad (7)$$

This type of observer is designed to estimate both speed and load torque using the stator current quadrature and the machine's calculated speed equations, under the assumption that the load torque remains constant between sampling intervals. The state variable equation is given as follows:

$$\begin{cases} \frac{dx}{dt} = A \cdot x + B \cdot u \\ y = C \cdot x \end{cases} \quad (8)$$

with  $x = [w \ C_r]^T$ ,  $u = i_q$ ,  $A = \begin{bmatrix} -\frac{f}{J} & -\frac{1}{J} \\ 0 & 0 \end{bmatrix}$ ,  $B = \begin{bmatrix} \frac{3 \cdot p \cdot \psi_f}{J} \\ 0 \end{bmatrix}$ ,  $C = [1 \ 0]$ .

The following system state variables express the LO as the two blocks illustrated in Figure 2.

$$\begin{cases} \frac{d\hat{x}}{dt} = A \cdot \hat{x} + B \cdot u + L \cdot (y - \hat{y}) \\ \hat{y} = C \cdot \hat{x} \end{cases} \quad (9)$$

with:  $\hat{x} = [\hat{w} \ \hat{C}_r]^T$ ,  $L = \begin{bmatrix} l_1 & 0 \\ 0 & l_2 \end{bmatrix}$ .

In equation (9),  $\hat{x}$  represents the observed state value and  $L$  denotes the observer gain matrix. By utilizing the prediction error output ( $y - \hat{y}$ ), observer's performance is adjusted proportionally with the gain matrix  $L$ . To elaborate, precise selection of the matrix  $L$  is crucial for ensuring optimal system response and stability. By imposing the two poles  $p_1$  and  $p_2$ , it becomes possible to set the dynamic observation. As a result, we obtain the model of the LO, expressed as follows:

$$\begin{cases} \frac{d\hat{w}}{dt} = -\frac{f}{J}\hat{w} - \frac{1}{J}\hat{C}_r + \frac{\frac{3}{2} \cdot p \cdot (\psi_f \cdot i_q)}{J} + l_1(w - \hat{w}) \\ \frac{d\hat{\theta}}{dt} = \hat{w} \\ \frac{d\hat{C}_r}{dt} = l_2(\theta - \hat{\theta}) \end{cases} \quad (10)$$

By positioning the poles correctly, the gains that the coefficients  $l_1$  and  $l_2$  relate to may be obtained by the observer. The reaction is quicker and the system is more noise-sensitive when the pole is closer to 0.

## Proposed speed sensorless control for IPMSM

### SC theory

In recent years, various nonlinear control systems have been proposed for electrical machinery, with SC techniques (SCTs) standing out as an innovative approach. SCTs offer key advantages such as strong disturbance rejection, ease of design, and guaranteed global stability for the system. SCT shares similarities with SMC, as both methods guide the system dynamics toward predetermined behaviors defined by the designer.

The development of an SCT controller follows a systematic process based on the concept of directed self-organization. The analytical design of aggregated regulators (ADAR) methodology is applied in the SCT design process, which requires the system model to be in a state-space form<sup>37</sup>:

$$\frac{dx}{dt} = f(x) + \sum_{i=1}^m g_i(x) u_i \quad (11)$$

Here,  $x$  is a vector of state variables, and  $u_i$  represents the control inputs for  $i = 1, 2, \dots, m$ . The function  $f(x)$  represents the natural (uncontrolled) dynamics of the system, which describe how the state variables evolve over time in the absence of control inputs. The term  $g_i(x)$  represents the influence of the control inputs  $u_i$  on the system's dynamics, dictating how the system responds to control actions. After determining the system's order and the number of control channels, the state variables are grouped into macro-variables, denoted as  $\Psi(x)$ , corresponding to each control input.

These macro-variables are designed to align with the control objectives.

Each macro-variable  $\Psi_i(x)$  delineates a manifold.

$$\Psi(x) = 0 \quad (12)$$

The set of all such manifolds constitutes an invariant manifold, described as:

$$\Psi_i(x) = 0 \quad (13)$$

This invariant manifold represents the desired operational states of the system, aligning with the control goals. To ensure the system converges toward the invariant manifold, it is governed by the following functional equation<sup>38</sup>:

$$T \frac{d\Psi_i}{dt} + \Psi_i = 0, T > 0 \quad (14)$$

This equation drives the system to approach the invariant manifold exponentially, with the time constant determined by  $T$ . The control laws  $u_i$  are derived by substituting the macro-variables  $\Psi(x)$  into equation (14), leading to control laws that depend on the system parameters, state variables, and the convergence time to the invariant manifold. Once the macro-variables are defined, the remainder of the SCT design process is purely algebraic.

### Designed ISO strategy

The integral-synergetic technique (IST) is a modified version of the SCT designed to enhance the robustness and characteristics of the classical technique. By adding integration to the classical SCT, the IST technique ensures increased efficiency and strategic effectiveness in enhancing system performance, particularly in enhancing the IPMSM characteristics. The following definition applies to the control legislation of the planned IST:

$$\Psi + T_1 \frac{d\Psi}{dt} + T_2 \int_0^t \Psi \cdot dt \quad (15)$$

where, the positive parameters for the derivative and integration sections are denoted by  $T_1$  and  $T_2$ , respectively.

Figure 3 showcases the IST. Upon comparing this novel technique with other nonlinear controls such as SMC or BC approach, it becomes evident that it is considerably simpler and more straightforward to implement. Moreover, this method merely necessitates knowledge of the surfaces; it does not mandate familiarity with the mathematical formulation of the system under investigation. As a result, it can be readily applied without the need for extensive computations or

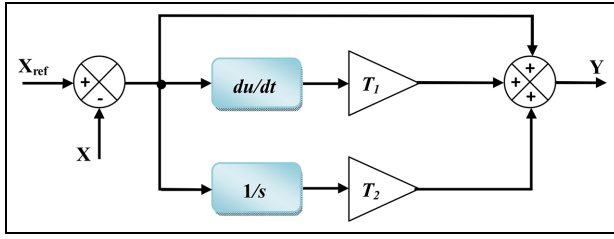


Figure 3. Block diagram of IST strategy.

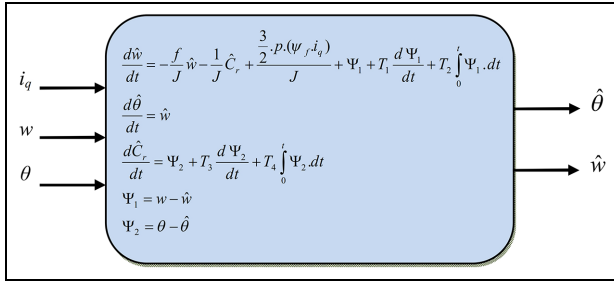


Figure 4. Block diagram of the proposed ISO technique.

knowledge of the system's mathematical form. The controller proposed in this study stands out from numerous scientific investigations due to its unique concept, principle, simplicity, and ease of use.

This paper introduces a novel ISO technique aimed at enhancing robustness and dynamic performance. In comparison to the LO, the ISO demonstrates greater robustness. Through the incorporation of derivative and integral terms of the macro-variable in its design, the designed observer not only exhibits fast dynamic response but also offers significant robustness against parameter uncertainties and disturbances. Furthermore, unlike the traditional synergetic technique, the IST ensures robustness throughout the system's entire response, starting from the initial time instant.

The design of the proposed observer is also based on the nonlinear model represented by equation (10), with

the modification of gains  $l_1$  and  $l_2$  by the new technique IST, illustrated in equation (15), as follows:

$$\begin{cases} \frac{d\hat{w}}{dt} = -\frac{f}{J}\hat{w} - \frac{1}{J}\hat{C}_r + \frac{\frac{3}{2} \cdot p \cdot (\psi_f \cdot i_q)}{J} + \Psi_1 + T_1 \frac{d\Psi_1}{dt} \\ \quad + T_2 \int_0^t \Psi_1 dt \\ \frac{d\hat{\theta}}{dt} = \hat{w} \\ \frac{d\hat{C}_r}{dt} = \Psi_2 + T_3 \frac{d\Psi_2}{dt} + T_4 \int_0^t \Psi_2 dt \end{cases} \quad (16)$$

With:

$$\Psi_1 = w - \hat{w} \quad (17)$$

$$\Psi_2 = \theta - \hat{\theta} \quad (18)$$

The schematic diagram of the suggested ISO is illustrated in Figure 4.

Figure 5 illustrates the suggested system block diagram, which incorporates field-oriented control (FOC) for efficient IPMSM management, along with a PWM strategy, and introduces the suggested speed estimation algorithm. The speed controller takes the speed reference  $w_{ref}$  as input and generates a torque command  $T_{com}$  to drive the motor at the desired speed. This torque command feeds into the FOC, which produces the reference current  $i_{dq}^*$ . The PI current controller then generates voltage commands  $v_{dq}^*$ , which are converted into 3-phase signals and supplied to the PWM converter. The actual stator current  $i_q$ , the real position  $\theta$  obtained from the position sensor, and  $w$ , derived from the real position's derivative, are used as inputs for the ISO. By applying the position and speed estimation

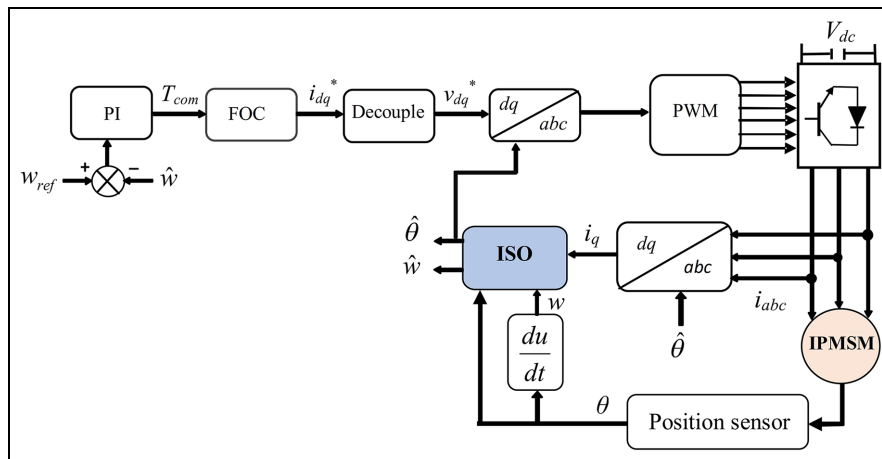


Figure 5. Proposed speed sensorless control system employing the ISO for IPMSM.

algorithm, the system in Figure 5 achieves sensorless speed control of the IPMSM.

### Stability analysis

The Lyapunov theorem will be used in this section to demonstrate the asymptotic stability of the closed-loop system when the proposed ISO is applied to sensorless speed control of IPMSM.

We consider  $V$  the positive Lyapunov function given in equation (19).

$$V = \frac{1}{2} \cdot \Psi_1^2 \quad (19)$$

where,  $\Psi_1$  is the tracking error defined in equation (17).

When deriving equation (19), equation (20) is obtained.

$$\frac{dV}{dt} = \Psi_1 \cdot \frac{d\Psi_1}{dt} \quad (20)$$

With:

$$\frac{d\Psi_1}{dt} = \frac{dw}{dt} - \frac{d\hat{w}}{dt} \quad (21)$$

Posing ( $\hat{C}_r - C_r \approx 0$ ) and according to equations (7) and (16), equation (21) becomes:

$$\begin{aligned} \frac{d\Psi_1}{dt} &= \frac{dw}{dt} - \frac{d\hat{w}}{dt} \\ &= -\frac{f}{J}\Psi_1 - \Psi_1 - T_1 \cdot \frac{d\Psi_1}{dt} - T_2 \int_0^t \Psi_1 dt \quad (22) \\ &= -\frac{f}{J}\Psi_1 - \Psi_1 - T_1 \cdot \frac{d\Psi_1}{dt} - T_2 \cdot \Psi_1 \cdot t \end{aligned}$$

After calculation, equation (22) becomes:

$$\frac{d\Psi_1}{dt} = \frac{1}{T_1 + 1} \left( -\frac{f}{J}\Psi_1 - \Psi_1 - T_2 \cdot \Psi_1 \cdot t \right) \quad (23)$$

By replacing equation (23) in equation (20), equation (20) can be written.

$$\frac{dV}{dt} = \frac{1}{T_1 + 1} \left( -\frac{f}{J}\Psi_1^2 - \Psi_1^2 - T_2 \cdot \Psi_1^2 \cdot t \right) \leq 0 \quad (24)$$

Where,  $T_1$  and  $T_2$  are positive parameters.

It can be observed that the derivative of the Lyapunov function is negative. Therefore, the asymptotic stability of the closed-loop system is guaranteed according to the Lyapunov theorem.

## Simulation results

Simulations were conducted under both steady-state and transient conditions to validate the proposed ISO. The performance of the observer was compared with that of the conventional LO, and the IPMSM parameters are listed in Table 2.

Using MATLAB/Simulink software, four simulation tests were conducted to demonstrate the IPMSM capacity to function in all conditions and assess the effectiveness of the observer methodologies examined in this research. The figures in the four condition displays several key parameters, including the real rotor speed, the estimated rotor speed, the reference speed, the stator current components ( $i_d$  and  $i_q$ ), the difference between the real and the estimated speed, as well as the electromagnetic torque.

In each test, three numerical values such as: IAE, ITAE, and ISE were calculated and compared for both the proposed observer and the conventional one. These values provide a clear indication of the superiority of the suggested observer in this study.

The expressions for IAE, ITAE, and ISE are given as follows:

$$IAE = \int_0^t |e(t)| dt \quad (25)$$

$$ITAE = \int_0^t |e(t)| \cdot t dt \quad (26)$$

$$ISE = \int_0^t (e(t))^2 dt \quad (27)$$

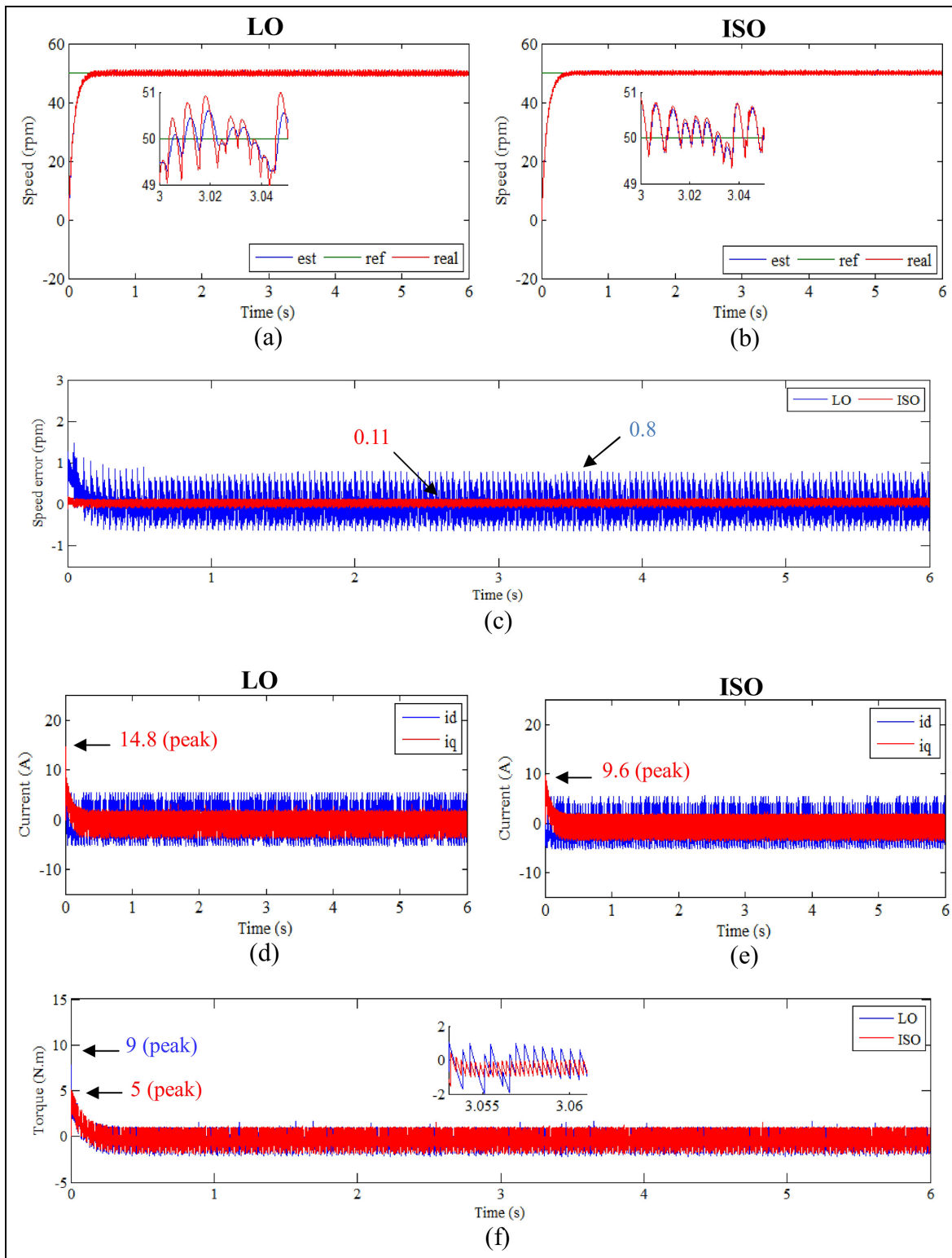
### First test

Figure 6 presents the simulation outcomes when the system is operating in low speed (50 rpm) and without

**Table 2.** IPMSM parameters.<sup>39</sup>

Parameter	Symbol	Value
Stator resistance	$R_s$	0.18 $\Omega$
Number of pole pairs	$p$	5
q-Axis inductance	$L_q$	0.29 mH
d-Axis inductance	$L_d$	0.174 mH
Inertia	$J$	0.067 kg/m <sup>2</sup>
Permanent-magnet flux linkage	$\psi_f$	0.0711 Wb
Rated speed	$N$	2000 rpm
Viscous friction coefficient	$f$	0.0003 Nm/rad.s <sup>-1</sup>
Rated current	$I_R$	150 A
DC-link voltage	$V_{dc}$	380 V
Switching frequency	$f_{sw}$	8 kHz
Rated torque	$T_R$	286 Nm





**Figure 6.** zFirst test results.

a load, employing both the conventional LO and the proposed ISO, where the speeds for both strategies follow the references well (Figure 6(a) and (b)). Also, the currents in the case of the two strategies take the same form, with zero value and ripples (Figure 6(d) and (e)). Figure 6(c) shows that when utilizing the LO, the maximum value reaches approximately 0.8rpm for speed

error curve under stable conditions. On the other hand, when implementing the ISO technique, it registers a peak value of approximately 0.11 rpm, resulting in a reduction of the speed error by approximately 0.69 rpm. This signifies an enhancement in error reduction of roughly 86.25%. Figure 6(f) demonstrates in the startup a small peak of ISO 5N.m torque



**Table 3.** Comparison of the IAE, ITAE, and ISE ratios between LO and ISO techniques for the first test.

Observer type	IAE	ITAE	ISE
LO	1.597	4.714	0.6599
ISO	0.6883	2.082	0.1595
Ratios (%)	56.90	55.83	75.82

compared to LO torque 9 N.m, the same goes for the stream of current  $i_q$  in Figure 6(d) and (e), where a startup of a high current estimated at 14.8 A for LO compared to ISO which is estimated at 9.6 A. these results indicate an improvement when the proposed observer was applied in reduction for startup current of roughly 35.13%.

Table 3 presents the IAE, ITAE, and ISE numerical values obtained when the conventional LO and the proposed ISO technique were utilized. The proposed observer achieved an enhancement in reduction estimated at 56.90% for IAE, 55.83% for ITAE, and 75.82% for ISE.

### Second test

Test two provides a comprehensive overview of the outcomes observed when the speed command is elevated from 2000 to 3000 rpm, at the 2-s and from 3000 to -2000 rpm the speed control increases the same goes for the current  $i_q$  which is an image of the torque. In Figure 7(a) and (b), the velocities closely follow the reference values for both control methods. However, the ISO shows a reduced error between the estimated and actual speed compared to the LO. Additionally, the currents in Figure 7(d) and (e) exhibit a similar pattern for both controls, with notable peaks for both LO and ISO at the speed change instants at 2 and 4 s. Moreover, the proposed ISO reduced these peaks by an estimated 41.53% compared to the LO.

An error between the real and estimated speed is illustrated in Figure 7(c). According to this Figure, and at 2 s, it's noteworthy that the speed error when using the LO stands at 2.12 rpm while utilizing the ISO a reduced speed error of 0.72 rpm. This indicates an error improvement of around 66.03%. In addition, when the machine's direction of rotation changes at 4 s, a significant peak is observed in the speed error curve (-10.8 rpm) for the LO, while this peak is substantially reduced for the proposed ISO (-5 rpm), indicating a reduction of 53.7%. The currents and torque are shown in Figure 7(d)-(f), respectively, with the figures demonstrating that the torque and current  $i_q$  share a similar pattern. Notably, some peaks are observed in these figures, particularly at the moments of speed change, where the peaks are lower for the proposed observer compared to the conventional one.

Table 4 displays the numerical values for IAE, ITAE, and ISE obtained using both the conventional

LO and the proposed ISO technique. The proposed observer demonstrated significant improvements, achieving reductions of approximately 54.94% for IAE, 53.06% for ITAE, and 85.24% for ISE. These results highlight the superior performance of the ISO in minimizing tracking errors and enhancing overall control accuracy, particularly in reducing cumulative errors and transient peaks. This improved efficiency not only ensures smoother operation but also contributes to greater stability and robustness of the system under varying conditions.

### Third test

Test three compiles the simulation outcomes under the circumstance where the load torque experienced an increase from 0 to 200 Nm at 3 s. It illustrates the system's remarkable control performance, attributed to its precise and high-speed regulation. The speeds follow the references well for the two applied observers, as illustrated in Figure 8(a) and (b). Nevertheless, the effect of the application of load is clear for the LO compared to the proposed ISO.

The currents in Figure 8(d) and (e) have the same form of change for the two used observers with the presence of ripples, where at the moment 3 s it is observed that the value of the current  $i_q$  increases as a result of the increase in the value of the torque at that moment. Figure 8(c) further presents data on speed errors. In the context of the LO, a speed error denoted amounts to -0.2 rpm at the moment when the load was applied. Conversely, within the ISO, the speed error is approximately -0.135 rpm. This translates to an improvement in error reduction of approximately 32.5%. In Figure 8(f), the shape of the torque change in the case of the two strategies is shown. This torque takes the form of a change in the current  $i_q$  with the presence of ripples, as these ripples are less if the ISO is used compared to the LO technique.

Table 5 presents the numerical values for IAE, ITAE, and ISE obtained using both the conventional LO and the proposed ISO technique. The proposed observer demonstrated substantial improvements, with reductions of approximately 89.54% for IAE, 93.55% for ITAE, and 98.22% for ISE. Based on this third test, it can be concluded that the proposed ISO is more effective at minimizing the impact of external disturbances, such as load application, compared to the conventional LO.

### Fourth test

The primary necessities were to ascertain whether there had been alterations in the parameters or if the parameter values listed in the IPMSM datasheet were inaccurate. This was accomplished by comparing the outcomes while varying the  $R_s$  by 100% and the  $L_d$  and  $L_q$  by 50%.

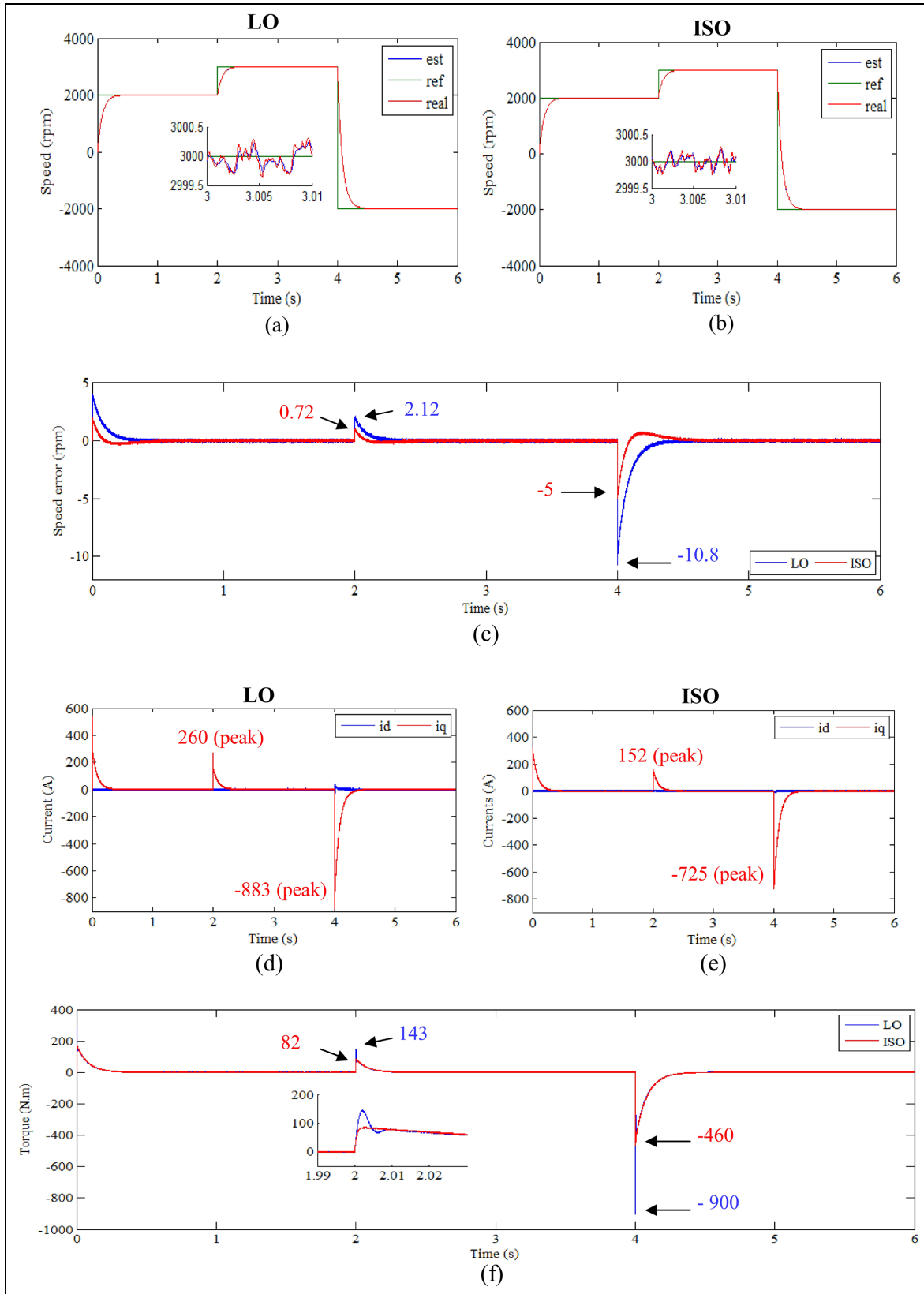


Figure 7. Second test results.

These fluctuations visibly impact the stator current, torque, and speed, with the speed error of the LO method exceeding that of the proposed ISO technique (Figure 9). Figure 9(a) and (b) represent speed changes

in the two-control cases, where this speed follows the reference well with a fast dynamic response. Specifically, the speed error amounts to roughly 1.4rpm when using the LO method, whereas with the

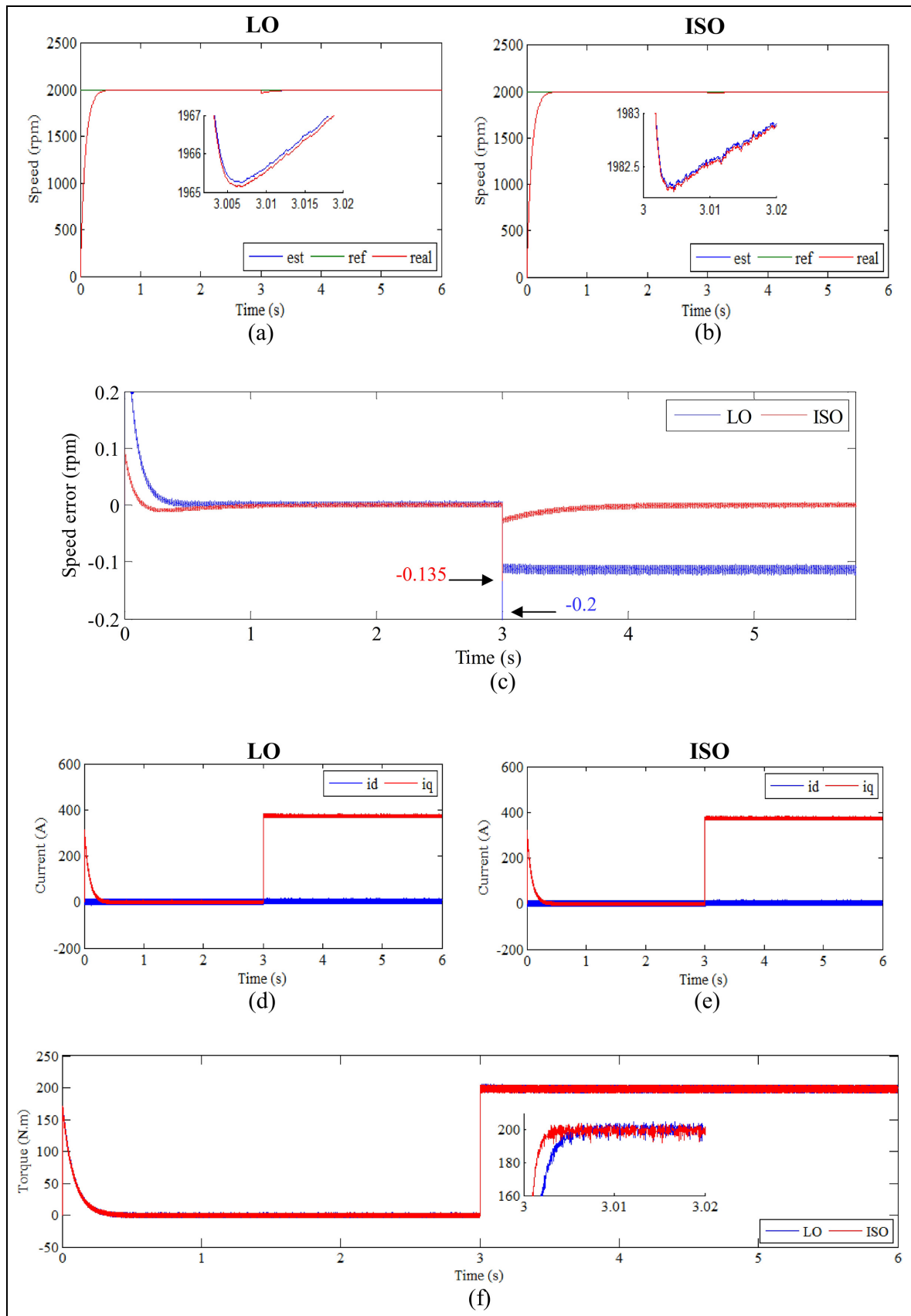


Figure 8. Third test results.

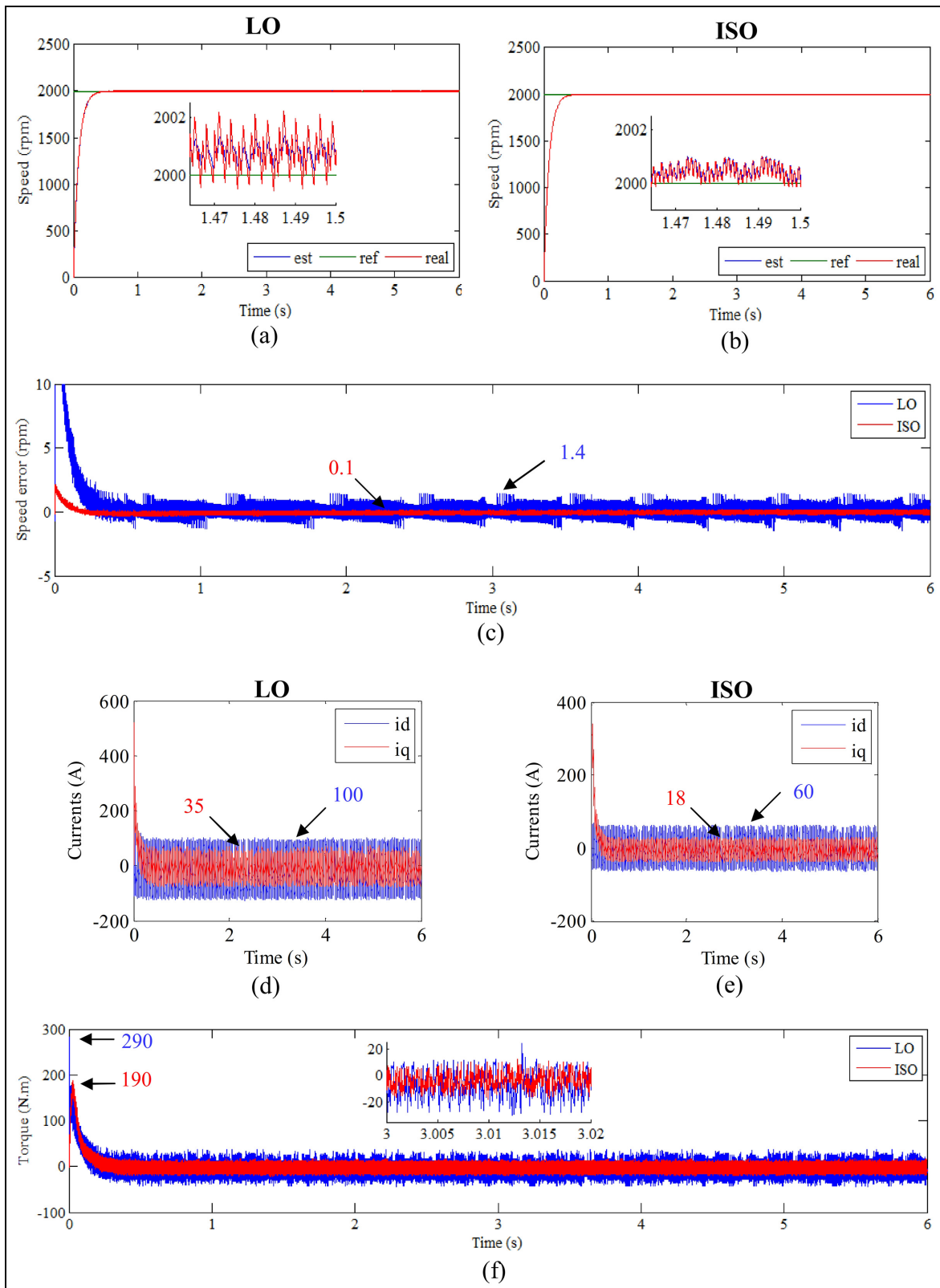


Figure 9. Fourth test results.

ISO implementation, it reduces to approximately 0.1 rpm. This indicates an error reduction of approximately 92.85%. Therefore, it can be inferred that the ISO approach exhibits greater robustness compared to the traditional LO technique (see Figure 9(c)).

Figure 9(d) and (e) show the currents  $i_d$  and  $i_q$  for the two controls, as these two currents have the same shape in the case of the two controls with the presence of high ripples when LO is used. These currents ripples are significantly reduced when the proposed ISO is used. The

**Table 4.** Comparison of the IAE, ITAE, and ISE ratios between LO and ISO techniques for the second test.

Observer type	IAE	ITAE	ISE
LO	1.311	3.72	4.775
ISO	0.5907	1.746	0.7046
Ratios (%)	54.94	53.06	85.24

**Table 5.** Comparison of the IAE, ITAE, and ISE ratios between LO and ISO techniques for the third test.

Observer type	IAE	ITAE	ISE
LO	0.3818	1.554	0.04557
ISO	0.03992	0.1001	0.00081
Ratios (%)	89.54	93.55	98.22

**Table 6.** Comparison of the IAE, ITAE, and ISE ratios between LO and ISO techniques for the fourth test.

Observer type	IAE	ITAE	ISE
LO	0.39	0.25	0.639
ISO	0.062	0.17	0.017
Ratios (%)	84.10	32	97.33

**Table 7.** Comparative outcomes derived from the proposed method in contrast to the conventional one.

Performance criteria	Conventional LO technique	Proposed ISO strategy
Dynamic responses	Medium	Fast
Speed variation effect	High	Low
Overshoot	Medium	Neglected
Settling time	High	Low
Rise time	High	Low
ITAE	High	Low
ISE	High	Low
IAE	High	Low
Precision	Medium	High
Parameters variation sensitivity	High	Low

torque curve is represented in Figure 9(f), where the shape of its change is the same as the shape of the change in current  $i_q$  with the presence of ripples, as these ripples are less if the proposed strategy is used.

The ISO surpasses LO in terms of rapid convergence and disturbance estimation, as evidenced by Figure 9(d)–(f). Across all tests, it is observed that the proposed strategy yields a smaller amplitude for the signals in the initial stages of current and torque compared to the conventional technique.

The numerical values of IAE, ITAE, and ISE obtained using both the LO and the ISO techniques are presented in Table 6. The ISO proves significant improvements, with reductions of approximately 84.10% in IAE, 32% in ITAE, and 97.33% in ISE. From this fourth test, it can be inferred that the proposed ISO is more efficient in minimizing the effects of internal disturbances, such as variations in machine parameters, compared to the LO.

Table 7 presents a comparative analysis between the proposed observer (ISO) and the conventional observer (LO). The results indicate notably favorable outcomes with the proposed approach, including enhanced dynamic responses, minimal sensitivity to speed variations, negligible overshoot, high precision, reduced rise and settling times, superior robustness, and lower values for ITAE, IAE, and ISE.

Table 8 summarizes the comparative quantitative performance metrics of the proposed observer and other techniques found in the literature. Simulation results indicate that the proposed ISO technique enhances control performance by minimizing speed drops at the moment the load is applied. It also reduces overshoot during changes in load torque or motor reference speed. Additionally, the ITAE is used as an evaluation criterion to compare the effects of various observer methods on overshoot and steady-state error. A lower ITAE value demonstrates that the proposed observer algorithm tracks the reference speed more accurately than other advanced observer techniques.

## Conclusions

In this study, a speed sensorless control based on an ISO for IPMSM has been proposed and presented. The designed method treats the important negatives of the conventional LO approach such as robustness. The suggested ISO has the advantage of being more accurate, reliable, and easy to use; because it is simple to obtain the observer gain. Moreover, the stability of the closed-loop system has been demonstrated using the Lyapunov theorem when the proposed ISO technique is applied. Simulation results show that the designed

**Table 8.** Comparing the performance of some scientific works with the proposed observer.

References	Techniques	Overshoot (%)	Speed drop (%)	Settling time (s)	ITAE
Liu et al. <sup>40</sup>	MRAS	1.99	2.32	0.55	2.91
Liu et al. <sup>41</sup>	MRAS-FL-PI	1.74	1.74	0.35	1.82
Khanh and Anh <sup>42</sup>	FL-MRAS-PI	1.35	1.34	0.275	1.08
Proposed technique	ISO	0.025	0.75	0.5	0.17

ISO outperforms the LO in speed control performance under four conditions, improving the speed IAE by approximately 56.90% in the first test, 54.94% in the second, 89.54% in the third, and 84.10% in the final test. It also outperforms the reconstruct or in no-load conditions, speed fluctuation conditions, low-speed control, and load fluctuation conditions. ISO significantly improves errors in the presence of parameter variations.

In future research, the sensorless control system using the proposed ISO, as outlined in this paper, will be experimentally implemented on an IPMSM. The expected outcome is a sensorless speed control method employing ISO that can be effectively applied in electric vehicles, which often experience significant load fluctuations and motor parameter variations due to weather conditions and operating environments.

### Declaration of conflicting interests

The author(s) declared no potential conflicts of interest with respect to the research, authorship, and/or publication of this article.

### Funding

The author(s) received no financial support for the research, authorship, and/or publication of this article.


### Institutional Review Board statement


Not applicable.

### Informed consent statement

Not applicable.

### ORCID iDs

Soufyane Boudouani  <https://orcid.org/0000-0003-4974-0264>

Habib Benboughenni  <https://orcid.org/0000-0001-8253-4863>

### Data availability statement

Data sharing not applicable to this article as no datasets were generated or analyzed during the current study.

### References

- Zhu S, Hu Y, Liu C, et al. Shaping of the air gap in a V-typed IPMSM for compressed-air system applications. *IEEE Trans Magn* 2021; 57(2): 1–5.
- Xu R and Tong W. Multi-objective hierarchical optimization of interior permanent magnet synchronous machines based on rotor surface modification. *CES Trans Electr Mach Syst* 2022; 6(4): 352–358.
- Wilcken N and Grotjahn M. Rotor position estimation for permanent magnet synchronous machines using electromotive force and anisotropy using extended-Kalman filter. *Forschung Ingenieurwesen* 2023; 87(2): 767–776.
- Kim ST, Yoon IS, Jung SC, et al. Robust sensorless control of interior permanent magnet synchronous motor using deadbeat extended electromotive force observer. *Energies* 2022; 15(20): 7568.
- Petro V and Kyslan K. Sensorless control of pmsm in low speed region using HF pulse signal injection method. *Acta Electrotech Inform* 2022; 22(1): 18–23.
- Chen Z and Liu Y. Sensorless control of marine permanent magnet synchronous propulsion motor based on adaptive extended Kalman filter. *Front Energy Res* 2022; 10: 1037595. DOI: 10.3389/fenrg.2022.1037595.
- Benaicha S. Robust sensorless speed control of an induction motor drive using a synergetic approach. *Revue Roumaine des Sciences Techniques-Série Électrotechnique et Énergétique*. 2023; 68(4): 381–387.
- Yang W, Guo H, Sun X, et al. Wide-speed-range sensorless control of IPMSM. *Electronics* 2022; 11(22): 3747.
- Zhu L, Xu B and Zhu H. Interior permanent magnet synchronous motor dead-time compensation combined with extended Kalman and neural network bandpass filter. *Prog Electromagn Res M* 2020; 98: 193–203.
- Liu X, Li Q, Wang L, et al. Data-driven state of charge estimation for power battery with improved extended Kalman filter. *IEEE Trans Instrum Meas* 2023; 72: 1–10.
- Niu H, Liu L, Jin D, et al. High-tracking-precision sensorless control of PMSM system based on fractional order model reference adaptation. *Fract Fraction* 2022; 7(1): 21.
- Elhaj A, Alzayed M and Chaoui H. Multiparameter estimation-based sensorless adaptive direct voltage MTPA control for IPMSM using fuzzy logic MRAS. *Machines* 2023; 11(9): 861.
- Ding L, Li YW and Zargari NR. Discrete-time SMO sensorless control of current source converter-fed PMSM drives with low switching frequency. *IEEE Trans Ind Electron* 2021; 68(3): 2120–2129.
- Zuo Y, Lai C and Iyer KLV. A review of sliding mode observer based sensorless control methods for PMSM drive. *IEEE Trans Power Electron* 2023; 38(9): 11352–11367.
- Wang F, He L, Kang J, et al. Adaptive model predictive current control for PMLSM drive system. *IEEE Trans Ind Electron* 2023; 70(4): 3493–3502.
- Qiu Z, Hu S and Liang X. Disturbance observer based adaptive model predictive control for uncalibrated visual servoing in constrained environments. *ISA Trans* 2020; 106: 40–50.
- Bakhti M, Ben Tarla L, Badr Bououlid I, et al. Mode Observer based adaptive model predictive control for a disturbed flexible manipulator active vibration control, 2024, vol 1141, pp.319–333.
- Wang M, Xu Y and Zou J. Sensorless control for permanent magnet synchronous motor based on ESO-PLL. *Proc CSEE* 2022; 42: 7599–7608.
- Xu W, Qu S and Zhang C. Fast terminal sliding mode current control with adaptive extended state disturbance observer for PMSM system. *IEEE J Emerg Sel Top Power Electron* 2023; 11(1): 418–431.
- Sriprang S, Nahid-Mobarakeh B, Pierfederici S, et al. Flatness control with extended luenberger observer for PMSM drive. In: *IEEE transportation electrification conference and expo, Asia-Pacific (ITEC Asia-Pacific)*, June 2018.

21. Niazi M, Cao J, Sun X, et al. Learning-based design of Luenberger observers for autonomous nonlinear systems. *Math. OC*, 2023.
22. Luo Y, Yang K and Zheng Y. Luenberger observer-based model predictive control for six-phase PMSM motor with localization error compensation. *IRE Trans Ind Electron* 2023; 70(11): 10800–10810.
23. Luo R, Wang Z and Sun Y. Optimized Luenberger observer-based PMSM sensorless control by PSO. *Model Simul Eng* 2022; 2022: 1–17.
24. Li W, Liu J and Gong C. High-frequency response current direct demodulation method for sensorless control of interior permanent magnet synchronous motor drives. *J Power Electron* 2022; 22(5): 784–795.
25. Ding H, Qin X and Wei L. Sensorless control of surface-mounted permanent magnet synchronous motor using adaptive robust UKF. *J Electr Eng Technol* 2022; 17(5): 2995–3013.
26. Salman E and Yilmaz M. A novel sensorless control approach for IPMSM using extended flux based PI observer for washing machine applications. *Int J Control Autom Syst* 2023; 21(7): 2313–2322.
27. Wu K and Lin Y. Sensorless speed control of PMLSM via adaptive interconnected state observer. *Int J Control Autom Syst* 2022; 20(11): 3822–3831.
28. Chen J and Wu X. Stator flux oriented sensorless DTFC for IPMSMs using pseudo-random HF signal injection. *J Power Electron* 2023; 23(12): 1846–1855.
29. Jiang JF, Zhou XJ, Zhao W, et al. A fast integral sliding mode controller with an extended state observer for position control of permanent magnet synchronous motor servo systems. *Front Inf Technol Electron Eng* 2020; 21(8): 1239–1250.
30. Ye S. Fuzzy sliding mode observer with dual SOGI-FLL in sensorless control of PMSM drives. *ISA Trans* 2019; 85: 161–176.
31. Benbouhenni H. Synergetic control theory scheme for asynchronous generator based dual-rotor wind power. *J Electr Eng Electron Control Comput Sci* 2021; 7(25): 19–28.
32. Benbouhenni H, Bizon N, Thounthong P, et al. A new integral-synergetic controller for direct reactive and active powers control of a dual-rotor wind system. *Meas Control* 2024; 57(2): 208–224.
33. Saihi L and Bouter A. Robust sensorless sliding mode control of PMSM with MRAS and Luenberger extended observer. In: *8th international conference on modelling, identification and control (ICMIC-2016)*, Algiers, Algeria, 15–17 November 2016.
34. Zhao M, An Q, Chen C, et al. Observer based improved position estimation in field-oriented controlled PMSM with misplaced hall-effect sensors. *Energies* 2022; 15(16): 5985.
35. He L, Wang F, Wang J, et al. Zynq implemented Luenberger disturbance observer based predictive control scheme for PMSM drives. *IEEE Trans Power Electron* 2020; 35(2): 1770–1778.
36. Boulghasoul Z, Kandoussi Z, Elbacha A, et al. Fuzzy improvement on Luenberger observer based induction motor parameters estimation for high performances sensorless drive. *J Electr Eng Technol* 2020; 15(5): 2179–2197.
37. Boumegouas MKB, Kouzi K and Birame M. Robust synergetic control of electric vehicle equipped with an improved load torque observer. *Int J Emerg Electric Power Syst* 2024; 25(2): 197–205.
38. Wang X, Wei C, Chen Y, et al. Improved model-free synergetic control of permanent magnet synchronous motor using unknown input observer. *Meas Control* 2024; 57(8): 1112–1122.
39. Sun X, Xu N, Yao M, et al. Efficient feedback linearization control for an IPMSM of EVs based on improved firefly algorithm. *ISA Trans* 2023; 134: 431–441.
40. Liu X, Zhang G, Mei L, et al. Speed estimation with parameters identification of PMSM based on MRAS. *J Contr Autom Electr Syst* 2016; 27(5): 527–534.
41. Liu Y, Wan J, Li G, et al. MRAS speed identification for PMSM based on fuzzy PI control. In: *2009 4th IEEE conference on industrial electronics and applications*, 2009, pp.1995–1998. DOI: 10.1109/ICIEA.2009.5138552.
42. Khanh PQ and Anh HPH. Novel sensorless PMSM speed control using advanced fuzzy MRAS algorithm. *Arab J Sci Eng* 2022; 47(11): 14531–14542.

## Appendix

### Notation

IPMSM	Interior permanent magnet synchronous motor
AC	Alternative current
MRAS	Model reference adaptive system
MPC	Model predictive control
LO	Luenberger observer
SC	Synergetic control
FW	Field weakening
ADAR	Analytical design of aggregated regulators
PWM	Pulse width modulation
EF	Extended flux
IAE	Integral absolute error
ISE	Integral square error
ISO	Integral synergetic observer
EKF	Extended Kalman filter
SMO	Sliding mode observer
ESO	Extended state observer
IST	Integral synergetic technique
SMC	Sliding mode control
SCT	Synergetic control technique
FOC	Field-oriented control
HF	High-frequency
PI	Proportional-integral
ITAE	Integral time absolute error
LQR	Linear quadratic regulator